

# Modelling ultra-fast nanoparticle melting with the Maxwell–Cattaneo equation

Matthew G. Hennessy<sup>\*1</sup>, Marc Calvo-Schwarzwalder<sup>1,2</sup>, and Timothy G. Myers<sup>1,2</sup>

<sup>1</sup>*Centre de Recerca Matematica, Campus de Bellaterra, Edifici C, 08193 Bellaterra, Spain*

<sup>2</sup>*Departament de Matematiques, Universitat Politecnica de Catalunya, 08028 Barcelona, Spain*

December 14, 2024

## Abstract

The role of thermal relaxation in nanoparticle melting is studied using a mathematical model based on the Maxwell–Cattaneo equation for heat conduction. The model is formulated as a one-phase Stefan problem that includes heat transport through the liquid. The temperature across the solid-liquid interface is assumed to be continuous or have a jump determined by the Rankine–Hugoniot condition. The model is solved using asymptotic and numerical methods. The analysis shows that when realistic parameter values are used with the jump condition, nanoparticle melting can only begin at temperatures that greatly exceed the bulk melting temperature, contradicting experimental studies. Furthermore, the Fourier-based solution can only be recovered in the classical limit of zero relaxation time when the temperature is continuous across the solid-liquid interface. These results demonstrate that it is inappropriate to use the jump condition in models of phase change. Numerical investigations reveal that thermal relaxation can increase the time required to melt a nanoparticle by up to 500%. Thus, thermal relaxation is an important process to capture in models of nanoparticle melting and is expected to be relevant in other rapid phase-change processes.

**Keywords:** Nanoparticle, Stefan problem, non-Fourier conduction, Maxwell–Cattaneo, ultra-fast melting, jump condition

## 1 Introduction

Technological advancements are driving the need to better understand the thermal characteristics of nanosystems [1, 2]. Perhaps the simplest and most theoretically studied nanosystem is the spherical nanoparticle. The one-dimensional geometry of a nanoparticle is ideal for developing mathematical models which can be compared against experimental data and used to assess new theories of nanoscale heat transport and phase change. From a practical perspective, nanoparticles play fundamental roles in novel drug delivery systems [3], materials with modified properties [4, 5], and for improving the efficiency of solar collectors [6]. Many current and future applications of nanoparticles require quantitative knowledge of how they respond to their thermal environment and their behaviour during melting.

---

<sup>\*</sup>mhennessy@crm.cat

The thermal response of a nanoparticle differs from that of a macroscopic body for two main reasons. Firstly, the large ratio of surface to bulk atoms leads to many key thermophysical properties, such as melt temperature [7–9], latent heat [10–12], and surface energy [13] becoming dependent on the size of the nanoparticle. Secondly, the mechanism of thermal transport changes between the macroscale and the nanoscale. At the macroscale, heat is transported by a diffusive process that is driven by frequent collisions between thermal energy carriers known as phonons. Diffusive transport of heat across macroscopic length scales is well described by Fourier’s law. On nanometer length scales, thermal energy is transported by a ballistic process driven by infrequent collisions between phonons. The finite time between phonon collisions results in a wave-like propagation of heat with finite speed [14, 15]. Since Fourier’s law leads to an infinite speed of heat propagation, it is not suitable for describing ballistic energy transport.

Recent theoretical studies of nanoparticle melting have investigated the role of size-dependent material properties [16–22] using models that are derived from Fourier’s law. Consequently, these models can only capture the diffusive regime of thermal transport rather than the ballistic regime that is more relevant for nanosystems. These studies also predict that nanoparticle melting occurs on pico- to nanosecond time scales, which are of the same order as the time between phonon collisions in many metallic systems [14]. Thus, there is strong evidence to suggest that non-Fourier heat conduction should be accounted for in theoretical models of nanoparticle melting.

The observation of wave-like thermal transport in liquid helium [23] prompted the derivation of new models of heat conduction that avoid the infinite speed of heat propagation predicted by Fourier’s law. The first non-Fourier model of heat conduction was simultaneously proposed by Cattaneo [24] and Vernotte [25], who introduced a thermal relaxation time into Fourier’s law. Microscopically, the relaxation time reflects the time between phonon collisions; macroscopically, it represents a time lag between the imposition of a temperature gradient and the creation of a thermal flux. The model proposed by Cattaneo and Vernotte is sometimes called the Maxwell–Cattaneo equation due to the similarity with the equation derived by the British physicist when providing a mathematical basis for the kinetic theory of gases [26]. When the Maxwell–Cattaneo equation is combined with conservation of energy, the so-called hyperbolic heat equation for the temperature is obtained. The Maxwell–Cattaneo equation predicts that thermal energy is transported as a wave with finite speed, making it better suited than Fourier’s law for capturing the ballistic transport regime [27]. However, it can also lead to results which violate the laws of thermodynamics [28]. Extensions to the classical theory of irreversible thermodynamics have been proposed as a means of rationalising this issue [29] and used to derive a family of heat conduction models that generalise the Maxwell–Cattaneo equation [30].

The first studies that incorporated the Maxwell–Cattaneo equation into models of phase change focused on mathematical issues [31–33] such as the correct form of boundary condition at the interface where phase change occurs [34, 35]. Some authors proposed that the temperature should be continuous across the interface [32, 36], while others suggested that there should be jump in temperature due to the hyperbolic nature of the governing equations [35, 37, 38]. Numerical studies based on one-dimensional Cartesian geometries showed that non-Fourier heat conduction affects the dynamics of phase change on time scales that are commensurate with the relaxation time of the material [39, 40]. Subsequent studies used the Maxwell–Cattaneo equation to model rapid solidification problems relating to dendrite formation in metal baths [41], pulsed-laser surface treatment [42], cryopreservation [43, 44], and cryosurgery of lung cancer [45]. In all of these works, the governing equations are solved using numerical methods. In fact, it

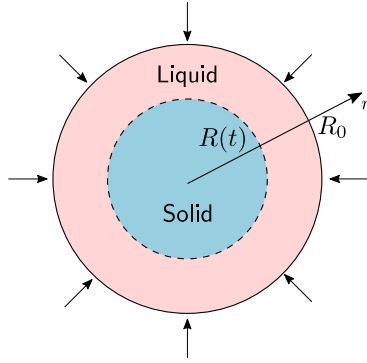


**Figure 1:** Spherically symmetry nanoparticle melting. The melting process is driven by an influx of thermal energy from the environment. The combined radius of the solid-liquid system is  $R_0$  and assumed to be constant. The position of the solid-liquid interface is denoted by  $R(t)$ .

appears that little attention has been given to seeking analytical or asymptotic solutions to non-Fourier models of phase change. One exception is the recent work by Hennessy *et al.* [46], who carried out a detailed asymptotic analysis of a non-Fourier model of solidification that accounts for the mean free path of phonons. The authors showed that non-classical transport mechanisms lead to additional time regimes, each with distinct solidification kinetics.

In this paper, we investigate the role of non-Fourier heat conduction and thermal relaxation in nanoparticle melting using a mathematical model based on the Maxwell–Cattaneo equation. Furthermore, we address the issue of which boundary condition should be imposed at the solid-liquid interface. Unlike many previous works which focus on solving the governing equations numerically, we use a combination of asymptotic and numerical methods to study the dynamics of phase change. The asymptotic analysis uncovers key shortcomings of the jump boundary condition for the temperature, one of which results in unrealistically high melting temperatures that contradict several experimental findings. An asymptotically reduced model is obtained in the limit of large Stefan number. To the best of our knowledge, this is the first time that such a reduction has been carried out on a model that is based on the Maxwell–Cattaneo equation. Finally, we assess the validity of our model in the context of classical thermodynamics.

The paper is organised as follows. In Section 2, a theoretical model for spherical nanoparticle melting is developed. The numerical scheme is presented in Section 3. Asymptotic solutions under different limiting situations are computed in Section 4. A discussion based on the results then follows in Section 5. The paper concludes in Section 6.

## 2 Model

We consider the transient melting of a spherical nanoparticle of radius  $R_0$  that is suspended in a warm environment held at temperature  $T_e$ . The transfer of heat from the environment into the nanoparticle initiates and sustains melting. The entire melting process is assumed to be symmetric so that it is sufficient to consider a one-dimensional model involving time  $t$  and the spherical radial coordinate  $r$ . The radial position of the solid-liquid interface, or melt front, is given by  $r = R(t)$ . Figure 1 illustrates this situation.

To enable the identification of the dominant mechanisms of phase change, the density variation that

occurs during melting is assumed to be so small that the change in total volume of the liquid-solid system and the motion of liquid can be neglected. As will be shown in Section 2.5, this assumption is reasonable for many metals. Density-driven motion and expansion of the liquid are considered in Refs. [18, 21]. We make a further simplifying assumption that the system can be described using a one-phase model that only includes heat conduction through the liquid. Consequently, the temperature of the solid  $T_s$  is assumed to be equal to the size-dependent melting temperature  $T_m(R)$  and the flux through the solid  $q_s$  is taken to be zero. As shown by Myers and Font [20], where thermal transport in a melting nanoparticle is modelled using Fourier’s law, this form of the one-phase model provides an excellent approximation to the full two-phase model. In particular, setting the solid temperature equal to the size-dependent melting temperature  $T_m(R)$  instead of the initial melting temperature  $T_m(R_0)$ , the latter of which is used in standard one-phase reductions, is crucial for achieving accurate solutions. In the one-phase model, it is assumed that the initial temperature of the solid is equal to the initial melting temperature  $T_m(R_0)$ . If the solid is below the initial melting temperature, then a two-phase model is required to describe the process of heating the solid to the initial melting temperature. Even after the onset of melting, heat conduction through the solid may be important and need to be captured by a two-phase model.

## 2.1 Bulk equations

The temperature  $T_s$  and thermal flux  $q_s$  of the solid are assumed to be

$$T_s(r, t) = T_m(R), \quad q_s(r, t) = 0. \quad (1)$$

Conservation of energy in the liquid is given by

$$\rho_l \frac{\partial u_l}{\partial t} + \frac{1}{r^2} \frac{\partial}{\partial r} (r^2 q_l) = 0, \quad (2)$$

where  $\rho_l$  is the density,  $u_l$  is the internal energy per unit mass, and  $q_l$  is the thermal flux. The size-dependent melting temperature and internal energies per unit mass will be defined below. The conduction of heat through the liquid is described by the Maxwell–Cattaneo equation. Thus, the thermal flux satisfies

$$\tau_r \frac{\partial q_l}{\partial t} + q_l = -k_l \frac{\partial T_l}{\partial r}, \quad (3)$$

where  $\tau_r$  is the thermal relaxation time and  $k_l$  is the thermal conductivity. The first term on the left-hand side of (3) captures the delayed response of the flux to a change in thermal environment. This delay is caused by the finite time between the interactions of heat carriers. The introduction of a time derivative in (3) leads to the flux depending on the history, *i.e.* the time integral, of the temperature gradient. For  $t \gg \tau_r$ , the memory term is negligible, implying that Fourier’s law is recovered on time scales that are large compared to the thermal relaxation time.

The internal energy of the solid and liquid per unit mass can be defined as

$$u_s = c_s(T_m - T_m^*), \quad u_l = c_l(T_l - T_m^*) + L_m, \quad (4)$$

where  $c_s$  and  $c_l$  are the heat capacities of the solid and liquid at constant pressure, respectively;  $T_l$  is the temperature of the liquid;  $T_m^*$  is the bulk melting temperature; and  $L_m$  is the latent heat of melting. The size-dependent melt temperature  $T_m$  is given by the standard form of the Gibbs–Thomson condition,

$$T_m(R) = T_m^* \left( 1 - \frac{l_{\text{cap}}}{R} \right), \quad (5)$$

where  $l_{\text{cap}}$  is the capillary length, *i.e.*, the length scale on which surface energy becomes important. The capillary length can be written as  $l_{\text{cap}} = (2\sigma_{sl})/(\rho_s L_m)$ , where  $\sigma_{sl}$  is the surface energy of the solid-liquid interface and  $\rho_s$  is the density of the solid. The standard heat equation can be obtained from (2) using the thermodynamic relationship  $du_l = c_l dT_l$ , which is valid for incompressible liquids (see Ref. [47, Chap. 2.3]), leading to

$$\rho_l c_l \frac{\partial T_l}{\partial t} + \frac{1}{r^2} \frac{\partial}{\partial r} (r^2 q_l) = 0. \quad (6)$$

## 2.2 Boundary conditions

The transfer of heat from the environment into the nanoparticle is modelled by a generalisation of Newton's law that accounts for the time scale of thermal relaxation. Relaxation effects can be incorporated into Newton's law by introducing a time derivative of the thermal flux [48, 49], leading to

$$\tau_r \frac{\partial q}{\partial t} + q = -h(T_e - T), \quad r = R_0, \quad (7)$$

where  $h$  is a heat transfer coefficient. Assuming that the Maxwell–Cattaneo equation holds at the surface, Eqns. (3) and (7) can be combined into a classical form of Newton's law given by

$$-k \frac{\partial T}{\partial r} = -h(T_e - T), \quad r = R_0. \quad (8)$$

It is important to note that the classical Newton boundary condition (8) only arises because of the specific forms of the non-classical Newton condition (7) and the Maxwell–Cattaneo equation (3); it could not have been imposed *a priori*. If an alternative model was used to describe non-Fourier heat conduction, then (8) would not be obtained.

Conservation of energy across the solid-liquid interface can be enforced by applying the Rankine–Hugoniot condition to the energy balance (2), yielding a Stefan condition given by

$$[\rho_l L_m + \rho_l c_l (T_l - T_m^*) - \rho_s c_s (T_m - T_m^*)] \frac{dR}{dt} = q_l, \quad r = R(t). \quad (9)$$

In deriving (9) we have used the definitions of the internal energies given by (4) and the solutions for the solid temperature and flux stated in (1).

The final boundary condition is the subject of some debate and, essentially, is determined by how the Maxwell–Cattaneo equation (3) is perceived. On one hand, the Maxwell–Cattaneo equation can be viewed in the same manner as Fourier's law as a constitutive relationship that is independently applied to the solid and liquid phases. In this case, it is natural to require the temperature to be continuous across the solid-liquid interface [32, 36], leading to the boundary condition

$$T_l = T_m(R), \quad r = R(t). \quad (10)$$

The condition (10) is consistent with classical formulations of phase-change problems based on Fourier's law. On the other hand, the Maxwell–Cattaneo equation can be viewed as a physical law that must hold throughout the two-phase mixture. In this case, it is natural to apply the Rankine–Hugoniot condition to (3), which leads to a jump condition for the temperature [35, 37, 38]

$$k_l T_l - k_s T_m(R) = \tau_r q_l \frac{dR}{dt}, \quad r = R(t). \quad (11)$$

A potentially problematic aspect of (11) is that naively taking  $\tau_r \rightarrow 0$  only recovers temperature continuity at the melt front when the solid and liquid have equal thermal conductivities, which not the case for most materials. We will explore the limit  $\tau_r \rightarrow 0$  in greater detail in Section 4.2 using asymptotic methods.

Assuming that temperature continuity (10) is true, then the Stefan condition (9) and the Gibbs–Thomson condition (5) can be combined to obtain

$$\left[ \rho_l L_m - \frac{(\rho_l c_l - \rho_s c_s) T_m^* l_{\text{cap}}}{R} \right] \frac{dR}{dt} = q_l, \quad r = R(t). \quad (12)$$

The reduced form of the Stefan condition (12) shows that it is possible to define a size-dependent effective latent heat given by  $L_{\text{eff}}(R) = L_m - [\rho_l c_l - (\rho_s/\rho_l)c_s] T_m^* l_{\text{cap}}/R$ . Since the heat capacity of a liquid is generally greater than that of the corresponding solid, the effective latent heat becomes zero at a critical radius  $R_{\text{crit}}$  defined by

$$R_{\text{crit}} = \left[ \frac{(\rho_l c_l - \rho_s c_s) T_m^*}{\rho_l L_m} \right] l_{\text{cap}}. \quad (13)$$

At this critical radius, no additional energy is required to melt the solid core, so the nanoparticle instantaneously transforms to liquid.

When the jump condition (11) is used in place of the continuity condition (10), the Stefan condition (9) and the jump condition (11) can be combined into a quadratic equation for the speed of the melt front  $dR/dt$ . The meaning of the two solutions of this equation are discussed in the context of shock propagation by Greenberg [35]. In this problem, the only admissible solution is that which leads to  $dR/dt < 0$  and is given by

$$[\rho_l L_m + \rho_l c_l (T_l - T_m^*) - \rho_s c_s (T_m - T_m^*)]^{1/2} \frac{dR}{dt} = - \left( \frac{k_l T_l - k_s T_m}{\tau_r} \right)^{1/2}, \quad r = R(t). \quad (14)$$

By solving for  $dR/dt$  in (14) and substituting the result into (11), a nonlinear relationship between the flux and temperature at the melt front is obtained,

$$[\rho_l L_m + \rho_l c_l (T_l - T_m^*) - \rho_s c_s (T_m - T_m^*)]^{1/2} (k_l T_l - k_s T_m)^{1/2} = -\tau_r^{1/2} q_l, \quad r = R(t). \quad (15)$$

When solving the problem with the jump condition using asymptotic methods in Section 4, the general form of the Stefan condition (9) will be used along with the nonlinear relationship (15). However, when solving the problem numerically using the approach described in Section 3, it is more convenient to use the jump condition (11), which is linear in the temperature and the flux, along with (14).

### 2.3 Initial conditions

Melting begins from the surface of the nanoparticle so that the initial position of the melt front is given by  $R(0) = 1$ . As this corresponds to a nanoparticle that is completely solid when  $t = 0$ , it is not possible to impose initial conditions for the temperature and flux of the liquid. However, as shown in Section 4.1, it is possible to obtain an asymptotic solution to the model that is valid for arbitrarily small times, which can be used in place of initial conditions.

### 2.4 Non-dimensionalisation

The governing equations are now cast into dimensionless form by a suitable rescaling of the variables. In doing so, we make the simplifying assumption that the model parameters are independent of temperature,

although it is straightforward to account for their temperature dependence. Spatial variables are scaled by the initial radius of the solid nanoparticle  $R_0$ . We let  $\Delta T = T_e - T_m(R_0)$  be the characteristic temperature scale of the system. As it is the influx of heat from the environment that drives the melting process, it is sensible to define a scale for the flux  $q$  using the Newton boundary condition (7); this leads to  $q \sim h\Delta T$ . Finally, a time scale is chosen by balancing the change in latent heat with the thermal energy that is delivered to the interface, giving  $t \sim (\rho_l L_m R_0)/(h\Delta T)$ . Using these scales, we define dimensionless variables, marked by hats, given by  $t = (\rho_l L_m R_0)/(h\Delta T)\hat{t}$ ,  $r = R_0\hat{r}$ ,  $R(t) = R_0\hat{R}(\hat{t})$ ,  $T_l = T_m(R_0) + (\Delta T)\hat{T}$ , and  $q_l = (h\Delta T)\hat{q}$ . The dimensionless bulk equations are given by (upon dropping the hats)

$$\beta^{-1}\frac{\partial T}{\partial t} + \frac{1}{r^2}\frac{\partial}{\partial r}(r^2 q) = 0, \quad (16a)$$

$$\gamma\frac{\partial q}{\partial t} + q = -\mathcal{N}^{-1}\frac{\partial T}{\partial r}, \quad (16b)$$

where  $\gamma = \mathcal{C}\beta^{-1}\mathcal{N}$  is the effective relaxation parameter, which is the product of the Cattaneo number  $\mathcal{C}$ , the inverse Stefan number  $\beta^{-1}$ , and the Nusselt number  $\mathcal{N}$ . These dimensionless numbers are defined as

$$\mathcal{C} = \frac{\tau_r k_l}{\rho_l c_l R_0^2}, \quad \beta = \frac{L_m}{c_l \Delta T}, \quad \mathcal{N} = \frac{h R_0}{k_l}. \quad (17)$$

The Cattaneo number represents the ratio of the thermal relaxation time scale to the classical thermal diffusion time scale. The Stefan number characterises the time scale of melting relative to heat conduction. Small values of the Stefan number are associated with fast melting processes. The Nusselt number describes the rate at which thermal energy is transferred to the nanoparticle compared to the rate at which it is transported away from the surface by conduction. Large Nusselt numbers characterise situations involving rapid surface heating, with an infinite Nusselt number describing the case of an instantaneous jump in surface temperature. The effective relaxation parameter  $\gamma$  therefore describes how the importance of thermal relaxation is affected by the time scales of thermal diffusion, melting, and heat transfer.

The dimensionless Gibbs–Thomson condition for the melt temperature reads

$$T_m(R) = \theta\ell\left(1 - \frac{1}{R}\right), \quad (18)$$

where  $\theta = T_m^*/\Delta T$  is the dimensionless bulk melting temperature and  $\ell = l_{\text{cap}}/R_0$  is the non-dimensional capillary length. In the case of temperature continuity across the melt front, the boundary condition

$$T = T_m(R), \quad r = R(t), \quad (19a)$$

is imposed. When applying the jump condition, a non-dimensional form of the nonlinear flux-temperature relationship (15) is imposed,

$$\mathcal{L}^{1/2}\left[T + \theta(1 - \ell) - k\theta\left(1 - \frac{\ell}{R}\right)\right]^{1/2} = -\gamma^{1/2}\mathcal{N}^{1/2}q, \quad r = R(t), \quad (19b)$$

where

$$\mathcal{L} = 1 + \beta^{-1}T - \theta\ell\beta^{-1}(1 - \rho c R^{-1}) \quad (20)$$

plays the role of an effective latent heat and  $k = k_s/k_l$ ,  $\rho = \rho_s/\rho_l$ , and  $c = c_s/c_l$  are the ratios of thermal conductivity, density, and specific heat, respectively. In both cases, the non-dimensional Stefan condition

(9) can be written as

$$\mathcal{L} \frac{dR}{dt} = q, \quad r = R(t). \quad (21)$$

The rescaled Newton boundary condition governing the influx of thermal energy is given by

$$\frac{\partial T}{\partial r} = \mathcal{N}(1 - T), \quad r = 1. \quad (22)$$

Finally, the initial condition for the position of the melt front is  $R(0) = 1$ .

## 2.5 Parameter estimation

We consider nanoparticles that have initial radii in the range of 10 nm to 100 nm. The lower bound of 10 nm ensures that the melting process can be described using continuum theory, which is thought to hold on length scales greater than 2 nm [50]. The material constants are based on tin, as this element is commonly used in experimental studies of nanoparticle melting [10, 51, 52], making parameter values readily available. However, we also provide parameter values for gold and lead in Table 1. Following Bachelors *et al.* [51], we take the surface energy of the solid-liquid interface to be  $\sigma_{sl} = 0.055 \text{ J/m}^2$ . The corresponding capillary length is  $l_{\text{cap}} = 0.26 \text{ nm}$ . Estimates of the thermal relaxation time of metallic systems typically range from  $10^{-12} \text{ s}$  to  $10^{-10} \text{ s}$  [41]. The heat transfer coefficient  $h$  is difficult to estimate due to its dependence on the environment that surrounds the nanoparticle. Using thermodynamic arguments, Ribera and Myers [21] state that the maximum value of the heat transfer coefficient is  $h_{\text{max}} = 4.7 \times 10^9 \text{ W}/(\text{m}^2 \cdot \text{K})$ . The largeness of  $h_{\text{max}}$  reflects the fact that it provides the closest approximation to the fixed-temperature boundary condition that is possible without instantly vapourising the nanoparticle. We restrict our attention to the case where  $h = h_{\text{max}}$  and leave exploring the melting behaviour for smaller values of the heat transfer coefficient as an area of future work.

The corresponding non-dimensional numbers for tin are  $c = 0.85$ ,  $\rho = 1.03$ , and  $k = 2.23$ . The Stefan number is given by  $\beta = (218 \text{ K})/\Delta T$  and will typically be large unless the temperature difference  $\Delta T$  is on the order of 100 K. The dimensionless bulk melting temperature  $\theta = (505 \text{ K})/\Delta T$  will have the same order of magnitude as the Stefan number. The dimensionless capillary lengths are small and range from  $\ell = 2.6 \times 10^{-3}$  to  $2.6 \times 10^{-2}$  as  $R_0$  decreases from 100 nm to 10 nm. The Nusselt number can be expressed in terms of the initial radius as  $\mathcal{N} = (0.157 \text{ nm}^{-1}) R_0$  and will range from  $\mathcal{N}_{\text{max}} = 1.57$  to 15.7. Rather than estimate the order of magnitude of the Cattaneo number  $\mathcal{C}$ , it is more enlightening to work directly with the effective relaxation parameter, which may be written as  $\gamma = (\tau_r h \Delta T)/(\rho_l L_m R_0)$ . Using the maximum heat transfer coefficient  $h_{\text{max}}$ ,  $\tau_r = 10^{-10} \text{ s}$ , and  $R_0 = 10 \text{ nm}$ , the effective relaxation parameter can be written in terms of the temperature difference as  $\gamma = (0.115 \text{ K}^{-1}) \Delta T$ . A value of  $\Delta T \simeq 10 \text{ K}$  is reasonable and would make the effective relaxation parameter  $O(1)$  in size. However, for tin nanoparticles that exceed 10 nm in radius or which have reduced heat transfer coefficients or thermal relaxation times, the effective relaxation parameter will be smaller.

## 3 Numerical method

The non-dimensional model (16)–(22) is numerically solved using a semi-implicit finite difference method on a staggered grid [53]. The transformation  $\xi = (r - R(t))/(1 - R(t))$  is used to map the growing domain  $R(t) \leq r \leq 1$  to a stationary domain  $0 \leq \xi \leq 1$ . The stationary domain is then discretised into

**Table 1:** Thermophysical parameter values for some materials [17, 21].

Material	$T_m^*$ [K]	$L_m^*$ [kJ/kg]	$\rho_s/\rho_l$ [kg/m <sup>3</sup> ]	$c_s/c_l$ [J/(kg·K)]	$k_s/k_l$ [W/(m·K)]	$\sigma_{sl}$ [J/m <sup>2</sup> ]
Tin	505	58.5	7180/6980	230/268	67/30	0.055
Gold	1337	63.7	19300/17300	129/163	317/106	0.27
Lead	600	23.0	11300/10700	128/148	35/16	0.05

cells of uniform size. Second-order central differences are used to approximate spatial derivatives. The temperature is calculated at cell edges while the flux is calculated at cell midpoints. By staggering the grid in this manner, the usual second-order finite-difference scheme for the heat equation is recovered in the limit of zero relaxation time. Linear interpolation and extrapolation are used to map quantities from one grid to another and to evaluate the flux at points that lie outside of the physical domain. Given known values of the position and speed of the melt front,  $R$  and  $dR/dt$ , the temperature and the flux are implicitly solved using a backwards Euler iteration. With the newly computed values for the flux and temperature, the Stefan condition (21) is used to evaluate  $dR/dt$ . The position of the melt front  $R$  is then updated using a forward Euler iteration. This approach leads to a decoupling of the melting and transport processes and avoids the need to solve a nonlinear system of equations at each time step.

## 4 Asymptotic analysis

Asymptotic methods are used to calculate analytical solutions to the governing equations under specific limits and simplifying assumptions. We first focus on calculating an approximate solution that is valid for arbitrarily small times. This solution can be used as a consistent initial condition when numerically simulating the model. Furthermore, the small-time solution gives key insights into the physical relevance of the jump condition for the temperature. We then examine the “classical” limit as  $\gamma \rightarrow 0$ , showing that the Fourier solution is only recovered in the case of a continuous temperature profile. Finally, we construct solutions that are valid in the limit of large Stefan number. Large Stefan numbers characterise phase-change processes that are slow compared to the rate of thermal diffusion. As this is the case in many physical scenarios and for a range of materials, the large-Stefan number limit is perhaps the most common approach for simplifying models of phase change. The relatively fast rate of thermal diffusion implies that on the time scale of melting, the temperature can be well approximated by its quasi-static profile. An analytical solution for the temperature can then often be obtained, which allows the problem to be reduced to a system of ordinary differential equations for position of the free boundary and, in the case of non-Fourier heat conduction [46], the thermal flux.

### 4.1 Solution for small times

The behaviour of the solution for small times can be determined by introducing an artificial small parameter  $\varepsilon \ll 1$  and then writing  $t = \varepsilon \bar{t}$ . It will also be convenient to use the Maxwell–Cattaneo equation (16b) to write the Newton condition (22) as

$$\gamma \varepsilon^{-1} \frac{\partial q}{\partial t} + q = -(1 - T), \quad r = 1. \quad (23)$$

Appropriate scales for the remaining variables are chosen using a balancing procedure that ensures the initial influx of thermal energy from the environment is captured by the model. To facilitate the

calculation, we will assume that all of the dimensionless parameters (aside from  $\varepsilon$ ) are  $O(1)$  in magnitude.

#### 4.1.1 Fourier conduction

Setting the effective relaxation parameter  $\gamma$  to zero recovers the classical formulation of the melting problem. By combining (16a) and (16b), where the latter is reduced to Fourier's law when  $\gamma = 0$ , we obtain the classical heat equation

$$\varepsilon^{-1} \mathcal{N} \beta^{-1} \frac{\partial T}{\partial t} = \frac{1}{r^2} \frac{\partial}{\partial r} \left( r^2 \frac{\partial T}{\partial r} \right), \quad (24)$$

subject to the boundary conditions (19a) and (22). The Stefan condition now reads

$$\varepsilon^{-1} \mathcal{L} \frac{dR}{dt} = -\mathcal{N}^{-1} \frac{\partial T}{\partial r}, \quad r = R(\bar{t}). \quad (25)$$

To capture the initial influx of energy, we must balance the left- and right-hand sides of the Newton condition (22), which implies that the temperature gradient and the flux must be  $O(1)$  in size. Using these facts in the Stefan condition (25) leads to the conclusion that  $1 - R = O(\varepsilon)$ . Therefore, we rescale the variables according to  $r = 1 - \varepsilon \bar{r}$ ,  $R = 1 - \varepsilon \bar{R}$ , and  $T = \varepsilon \bar{T}$ . After taking the limit  $\varepsilon \rightarrow 0$ , the heat equation (24) becomes  $\partial^2 \bar{T} / \partial \bar{r}^2 = 0$ , which is subject to the boundary conditions  $\partial \bar{T} / \partial \bar{r} = -\mathcal{N}$  at  $\bar{r} = 0$  and  $\bar{T} = -\theta \ell \bar{R}$  at  $\bar{r} = \bar{R}(\bar{t})$ . Upon solving for the temperature, the Stefan condition (25) reduces to

$$[1 - \beta^{-1} \theta \ell (1 - \rho c)] \frac{d\bar{R}}{d\bar{t}} = 1. \quad (26)$$

In terms of the original non-dimensional variables, the solution for small times is given by

$$T(r, t) = \mathcal{N}[r - R(t)] - \theta \ell [1 - R(t)], \quad (27a)$$

$$q(r, t) = -1, \quad (27b)$$

$$R(t) = 1 - [1 - \beta^{-1} \theta \ell (1 - \rho c)]^{-1} t. \quad (27c)$$

Importantly, (27b) shows that the thermal flux predicted by Fourier's law is  $O(1)$  in size and constant in time, which results in the linear melting kinetics given by (27c). The magnitude of the flux ultimately arises from the form of the Newton condition (23). Since thermal relaxation effects have been neglected, the surface flux, and hence the bulk flux, instantaneously attain  $O(1)$  values. As we will show in Section 4.1.2 and Section 4.1.3, this will not be the case when relaxation effects are included in the model.

For the remainder of the section, we will focus on obtaining small-time solutions for positive  $O(1)$  values of the effective relaxation parameter  $\gamma$ . We will therefore replace Fourier's law with the Maxwell–Cattaneo equation given by (16b) and use the full form of the Newton boundary condition (23).

#### 4.1.2 Maxwell–Cattaneo conduction with temperature continuity

Balancing terms in the Newton boundary condition (23) requires the flux to be  $O(\varepsilon)$  in size,  $q = \varepsilon \bar{q}$ . From the Stefan condition (21), the small magnitude of the thermal flux implies that the width of the melt region is  $O(\varepsilon^2)$ . Thus, we let  $r = 1 - \varepsilon^2 \bar{r}$  and  $R = 1 - \varepsilon^2 \bar{R}$ . The Gibbs–Thomson condition (18) then indicates that  $T = \varepsilon^2 \bar{T}$ . Using these rescaled variables in the governing equations and taking  $\varepsilon \rightarrow 0$  results in a significantly reduced model. Conservation of energy (16a) becomes  $\partial \bar{q} / \partial \bar{r} = 0$ , implying the

flux is only a function of time. The Maxwell–Cattaneo equation (16b) reduces to

$$\gamma \frac{d\bar{q}}{d\bar{t}} = \mathcal{N}^{-1} \frac{\partial \bar{T}}{\partial \bar{r}}. \quad (28)$$

The boundary conditions read

$$\gamma \frac{d\bar{q}}{d\bar{t}} = -1, \quad \bar{r} = 0, \quad (29a)$$

$$\bar{T} = -\theta\ell\bar{R}, \quad \bar{r} = \bar{R}(\bar{t}). \quad (29b)$$

Finally, the Stefan condition is

$$[1 - \beta^{-1}\theta\ell(1 - \rho c)] \frac{d\bar{R}}{d\bar{t}} = -\bar{q}, \quad \bar{r} = \bar{R}(\bar{t}). \quad (30)$$

We assume that there is no flux through the surface of the nanoparticle at time  $\bar{t} = 0$ . The initial conditions for this problem are therefore given by

$$\bar{q}(0, 0) = 0, \quad \bar{R}(0) = 0. \quad (31)$$

The solution to this problem, written in terms of the original dimensionless variables, is given by

$$T(r, t) = \mathcal{N}[r - R(t)] - \theta\ell[1 - R(t)], \quad (32a)$$

$$q(r, t) = -\gamma^{-1}t, \quad (32b)$$

$$R(t) = 1 - \frac{1}{2} [1 - \beta^{-1}\theta\ell(1 - \rho c)] \gamma^{-1}t^2. \quad (32c)$$

By accounting for thermal relaxation effects, the magnitude of the flux (32b) is now predicted to increase linearly with time. This is in stark contrast to the instantaneous change in the thermal flux that is observed when using Fourier’s law to describe heat conduction. The gradual change of the thermal flux in the case of Maxwell–Cattaneo conduction leads to substantially slower melting kinetics, which are now quadratic in time.

### 4.1.3 Maxwell–Cattaneo conduction with temperature jump

The rescaling of variables is similar to the case when the temperature is continuous across the melt front. In particular, the flux must still be  $O(\varepsilon)$  in magnitude to balance both sides of the Newton condition (23). However, the temperature scale is now determined from the jump condition (19b), which implies that  $T = O(1)$ . We therefore rescale the variables according to  $r = 1 - \varepsilon^2\bar{r}$ ,  $R = 1 - \varepsilon^2\bar{R}$ ,  $T = \bar{T}$ , and  $q = \varepsilon\bar{q}$ . Upon taking  $\varepsilon \rightarrow 0$ , the bulk equations becomes

$$\beta^{-1} \frac{\partial \bar{T}}{\partial \bar{t}} + \frac{\partial \bar{q}}{\partial \bar{r}} = 0, \quad (33a)$$

$$\frac{\partial \bar{T}}{\partial \bar{r}} = 0. \quad (33b)$$

The boundary conditions are given by

$$\gamma \frac{\partial \bar{q}}{\partial \bar{t}} = -(1 - \bar{T}), \quad \bar{r} = 0, \quad (34a)$$

$$\bar{T} = \theta(1 - \ell)(k - 1), \quad \bar{r} = \bar{R}(\bar{t}). \quad (34b)$$

The Stefan condition (21) can be written as

$$\left[1 + \beta^{-1}\bar{T} - \beta^{-1}\theta\ell(1 - \rho c)\right] \frac{d\bar{R}}{d\bar{t}} = -\bar{q}, \quad \bar{r} = \bar{R}(\bar{t}). \quad (35)$$

The solution to (33)–(35), subject to the initial conditions (31), can be written in terms of the original dimensionless variables as

$$T(r, t) = \theta(1 - \ell)(k - 1), \quad (36a)$$

$$q(r, t) = -\gamma^{-1} [1 - \theta(1 - \ell)(k - 1)] t, \quad (36b)$$

$$R(t) = 1 - \frac{1}{2} \left[ \frac{1 - \theta(1 - \ell)(k - 1)}{1 + \beta^{-1}\theta[(1 - \ell)(k - 1) - \ell(1 - \rho c)]} \right] \gamma^{-1} t^2. \quad (36c)$$

From (36b) and (36c), it is seen that thermal relaxation leads to a similar linear decrease in the flux and quadratic melting kinetics that were observed in the case of temperature continuity across the melt front. However, the temperature is now  $O(1)$  in magnitude and spatially uniform, with a value that is set by the jump condition at the melt front. This leads to the possibility of the liquid temperature exceeding the temperature of the environment, which would prevent the onset of melting. Indeed, an examination of (36c), which can be simplified using  $\ell \ll 1$ , reveals that melting will only be possible if the inequality  $\theta(k - 1) < 1$  is satisfied. In terms of dimensional quantities, this inequality places a lower limit on the external temperature that allows for melting,  $T_e > (k_s/k_l)T_m^*$ . In deriving this bound, we have used  $\Delta T = T_e - T_m(R_0) \simeq T_e - T_m^*$ . As seen from Table 1, the thermal conductivity of the solid phase of a material is generally greater than that of the liquid phase by a factor of two or more. This implies that the effective melting temperature  $(k_s/k_l)T_m^*$  of a nanoparticle exceeds the bulk melting temperature. This result contradicts the findings of several experimental studies [7, 54, 55], which consistently report nanoparticle melting at temperatures that are substantially lower than the bulk melting temperature. Thus, we can conclude that the jump condition for the temperature is not valid in the context of nanoparticle melting.

## 4.2 Limit of zero thermal relaxation time

We now examine the “classical” limit given by  $\gamma \rightarrow 0$  with all other parameters  $O(1)$  in size. We first assume that the temperature is continuous across the melt front and then consider the case of a temperature jump.

### 4.2.1 Temperature continuity

There are two key time regimes in the limit as  $\gamma \rightarrow 0$ . The first time regime,  $t = O(\gamma)$ , captures the quick thermal relaxation that occurs as thermal energy is being transferred to the nanoparticle. In the second time regime,  $t = O(1)$ , the flux has relaxed to its Fourier value and the classical nanoparticle melting problem is recovered.

The scaling for the first time regime is obtained by balancing the flux relaxation with the inflow of thermal energy from the environment, which yields  $q = O(\gamma^{-1}t)$ . In order to capture melting, the width of the liquid region must scale like  $1 - R = O(\gamma^{-1}t^2)$ . The temperature scale is determined from the Gibbs–Thomson condition (19a) as  $T = O(\gamma^{-1}t^2)$ . The only scale left to determine is that for time. By inserting rescaled variables into the Maxwell–Cattaneo equation (16b), the only sensible balance occurs when  $t = O(\gamma)$ . Thus, the first time regime is captured by writing  $t = \gamma\tilde{t}$ ,  $r = 1 - \gamma\tilde{r}$ ,  $R = 1 - \gamma\tilde{R}$ ,  $q = \tilde{q}$ ,

and  $T = \gamma\tilde{T}$ . After taking  $\gamma \rightarrow 0$ , the energy equation (16a) reduces to  $\partial\tilde{q}/\partial\tilde{r} = 0$ , implying the flux is constant in space. The Maxwell–Cattaneo equation becomes

$$\frac{d\tilde{q}}{d\tilde{t}} + \tilde{q} = \mathcal{N}^{-1} \frac{\partial\tilde{T}}{\partial\tilde{r}}. \quad (37)$$

Differentiating (37) with respect to  $r$  shows that the temperature satisfies Laplace’s equation. The boundary conditions for the temperature are given by  $\partial\tilde{T}/\partial\tilde{r} = -\mathcal{N}$  at  $\tilde{r} = 0$  and  $\tilde{T} = -\theta\ell\tilde{R}$  at  $\tilde{r} = \tilde{R}(\tilde{t})$ . Upon solving for the temperature and inserting the result into (37), we find that the flux and the position of the melt front satisfy the coupled system of equations

$$\frac{d\tilde{q}}{d\tilde{t}} + \tilde{q} = -1, \quad (38a)$$

$$[1 - \beta^{-1}\theta\ell(1 - \rho c)] \frac{d\tilde{R}}{d\tilde{t}} = -\tilde{q}, \quad (38b)$$

subject to  $\tilde{q} = \tilde{R} = 0$  when  $\tilde{t} = 0$ . The solution for the temperature, flux, and position of the melt front, written in terms of the original dimensionless variables, is given by

$$T(r, t) = \mathcal{N}[r - R(t)] - \theta\ell[1 - R(t)], \quad (39a)$$

$$q(r, t) = -[1 - \exp(-t/\gamma)], \quad (39b)$$

$$R(t) = 1 - \left[ \frac{t + \gamma \exp(-t/\gamma) - \gamma}{1 - \beta^{-1}\theta\ell(1 - \rho c)} \right]. \quad (39c)$$

As  $t \rightarrow 0$  with  $\gamma$  fixed, the solutions for the flux (39b) and the position of the melt front (39c) reduce to

$$q(r, t) \sim -\gamma^{-1}t, \quad R(t) \sim 1 - \frac{1}{2}\gamma^{-1} [1 - \beta^{-1}\theta\ell(1 - \rho c)]^{-1} t^2, \quad (40)$$

in agreement with the small-time limit of the non-Fourier model given in (32).

In the second time regime, defined by  $t = O(1)$ , the relaxation terms can be neglected and the variables do not need to be rescaled from their original dimensionless form. The Maxwell–Cattaneo equation (16b) therefore reduces to Fourier’s law. The matching conditions for the flux and the position of the melt front can be obtained from (39b) and (39c) in the limit  $\gamma \rightarrow 0$  with  $t$  fixed, yielding

$$q(r, t) \sim -1, \quad R(t) \sim 1 - [1 - \beta^{-1}\theta\ell(1 - \rho c)]^{-1} t, \quad (41)$$

which are precisely the small-time solutions to the Fourier model (27). Consequently, non-classical transport mechanisms do not enter the leading-order problem on  $O(1)$  time scales, implying that the classical, Fourier-based model is completely recovered when temperature continuity is imposed at the melt front.

#### 4.2.2 Temperature jump

As in the case of temperature continuity, there are relaxation- and diffusion-dominated time regimes defined by  $t = O(\gamma)$  and  $t = O(1)$ , respectively. Carrying out the balancing procedure described in Section 4.2.1 shows that the appropriate rescaling is given by  $t = \gamma\tilde{t}$ ,  $r = 1 - \gamma\tilde{r}$ ,  $R = 1 - \gamma\tilde{R}$ ,  $q = \tilde{q}$ , and  $T = \tilde{T}$ , where the temperature scale has been determined by balancing terms in the jump condition (19b). Taking the limit  $\gamma \rightarrow 0$  shows that the governing equations have the same form as (33)–(35), with the exception of the Newton condition, which now reads

$$\frac{\partial\tilde{q}}{\partial\tilde{t}} + \tilde{q} = -(1 - \tilde{T}), \quad \tilde{r} = 0. \quad (42)$$

In terms of the original non-dimensional variables, the solutions for the flux, temperature and position of the melting front in the first time regime are given by

$$T(r, t) = \theta(1 - \ell)(k - 1), \quad (43a)$$

$$q(r, t) = [\theta(1 - \ell)(k - 1) - 1] [1 - \exp(-t/\gamma)], \quad (43b)$$

$$R(t) = 1 - \frac{1 - \theta(1 - \ell)(k - 1)}{1 + \beta^{-1}\theta[(k - 1) - (k - \rho c)\ell]} [t + \gamma \exp(-t/\gamma) - \gamma]. \quad (43c)$$

If we let  $t \rightarrow 0$  for fixed  $\gamma$ , then the small-time solution (36) is retrieved.

In the second time regime defined by  $t = O(1)$ , the original dimensionless variables do not need to be rescaled and Fourier's law is recovered. However, in the limit as  $\gamma \rightarrow 0$  with  $t = O(1)$ , the jump condition (19b) reduces to

$$T = \theta\ell \left(1 - \frac{1}{R(t)}\right) + \theta(k - 1), \quad r = R(t), \quad (44)$$

which only corresponds to the classical boundary condition when  $k = 1$ . The matching conditions for this time regime are obtained from (43) by taking the limit  $\gamma \rightarrow 0$  for fixed  $t$ , which yields

$$q \sim -1 + \theta(1 - \ell)(k - 1), \quad R \sim 1 - \frac{1 - \theta(1 - \ell)(k - 1)}{1 - \beta^{-1}\theta\ell(k - \rho c) + \beta^{-1}\theta(k - 1)}t. \quad (45)$$

By looking at (27) we observe that the matching conditions coincide with the small-time solution to the classical formulation only for  $k = 1$ . Therefore, the classical, Fourier-based melting dynamics will not generally be recovered in the limit as  $\gamma \rightarrow 0$ , demonstrating another important inadequacy of the jump condition for the temperature.

### 4.3 Solution for large Stefan numbers

We now compute asymptotic solutions in the limit as  $\beta \rightarrow \infty$  with  $\gamma = O(1)$  in the case of a continuous temperature profile. We do not repeat the calculation for the case of a temperature jump due the unphysical nature of the model with this boundary condition. More specifically, for all of the materials listed in Table 1, the assumption of a large Stefan number leads to the (dimensional) external number  $T_e$  being smaller than the effective melting temperature  $(k_s/k_l)T_m^*$ . Therefore, melting is simply not possible in the case of a large Stefan number and a temperature jump at the melt front.

#### 4.3.1 Maxwell–Cattaneo conduction with temperature continuity

Before proceeding with the calculation, it is helpful to re-examine the sizes of the various non-dimensional numbers that appear in the model. The parameter  $\theta$  is of the same order of magnitude as the Stefan number, implying that  $\theta = O(\beta)$ . The dimensionless capillary length  $\ell$  is always small. We will make an additional assumption that  $\theta\ell = O(1)$  as  $\beta \rightarrow \infty$  so that the temperature at the melt front is  $O(1)$  during the majority of the melting process. For practical scenarios, where  $\Delta T$  is of the order of a few Kelvin or larger, this assumption will be true.

After neglecting terms of order  $\beta^{-1}$  from (16a), the flux  $q$  can be written as

$$q(r, t) = \frac{Q(t)}{r^2}, \quad (46)$$

where  $Q(t)$  is the volume-averaged flux defined as

$$Q(t) = \frac{1}{1 - R(t)} \int_{R(t)}^1 q(r, t) r^2 dr. \quad (47)$$

By inserting (46) into the Maxwell–Cattaneo equation (16b), multiplying by  $r^2$ , and then differentiating with respect to  $r$ , the temperature is found to satisfy Laplace’s equation. After solving this equation and applying the boundary conditions in (19a) and (22), the temperature profile is given by

$$T(r, t) = \theta \ell \left[ 1 - \frac{1}{R(t)} \right] + \frac{\mathcal{N}\{R(t) + \theta \ell [1 - R(t)]\}}{R(t) + \mathcal{N}[1 - R(t)]} \left[ \frac{1}{R(t)} - \frac{1}{r} \right]. \quad (48)$$

Upon substituting (46) and (48) into (16b), a differential equation for the mean flux  $Q$  is obtained,

$$\gamma \frac{dQ}{dt} + Q = - \frac{R + \theta \ell (1 - R)}{R + \mathcal{N}(1 - R)}. \quad (49a)$$

By substituting the solution for the flux (46) into the Stefan condition (21), the position of the melt front evolves according to

$$\left[ 1 - \frac{(1 - \rho c) \theta \ell}{\beta R} \right] \frac{dR}{dt} = \frac{Q}{R^2}. \quad (49b)$$

Although the second term on the left-hand side of (49b) can generally be neglected, it does not lead to additional complications and thus it is retained. An initial condition for  $Q$  can be obtained via a small-time analysis. Following the methodology of Section 4.1, we find that the small-time behaviour of  $Q$  and  $R$  is given by

$$Q(t) \sim -\gamma^{-1} t, \quad R(t) \sim 1 - \frac{1}{2} [1 - \beta^{-1} (1 - \rho c) \theta]^{-1} \gamma^{-1} t^2, \quad (50)$$

as  $t \sim 0$ . The limiting behaviour in (50) exactly coincides with the small-time behaviour of the full model, implying that the solution to (49) will be uniformly valid for all times. The equations in (49) along with (50) form a reduced model that can be used to easily study the melting dynamics of nanoparticles.

## 5 Results and discussion

The asymptotic analysis of Section 4.2 reveals that when the Maxwell–Cattaneo equation is used to model heat conduction, the predicted melting behaviour is strongly dependent on the choice of boundary condition applied at the melt front. This is true even when the effective relaxation parameter is small. To explore the difference in melting dynamics in further detail, we numerically solve the governing equations using both boundary conditions and a small value of the relaxation parameter. Carrying out simulations using both boundary conditions for the same parameter values requires the Stefan number to be small: the jump condition may only be imposed when the temperature difference is sufficiently (and unrealistically) large. Thus, we set  $R_0 = 10$  nm,  $\tau_r = 10^{-13}$  s, and  $\beta = 0.25$ , corresponding to  $\Delta T \simeq 873$  K, which leads to  $\gamma \simeq 0.10$ .

The results of the simulations are shown as lines in Fig. 2, which plots the evolution of the position of the melt front and the mean thermal flux defined in (47). Also shown are the results obtained using Fourier’s law. Although the temperature profiles will be discussed in detail below, it suffices to say here that they are qualitatively similar. The circles and diamonds in Fig. 2 denote the asymptotic predictions of the flux and position of the melt front given by (39) and (43), respectively, which accurately capture

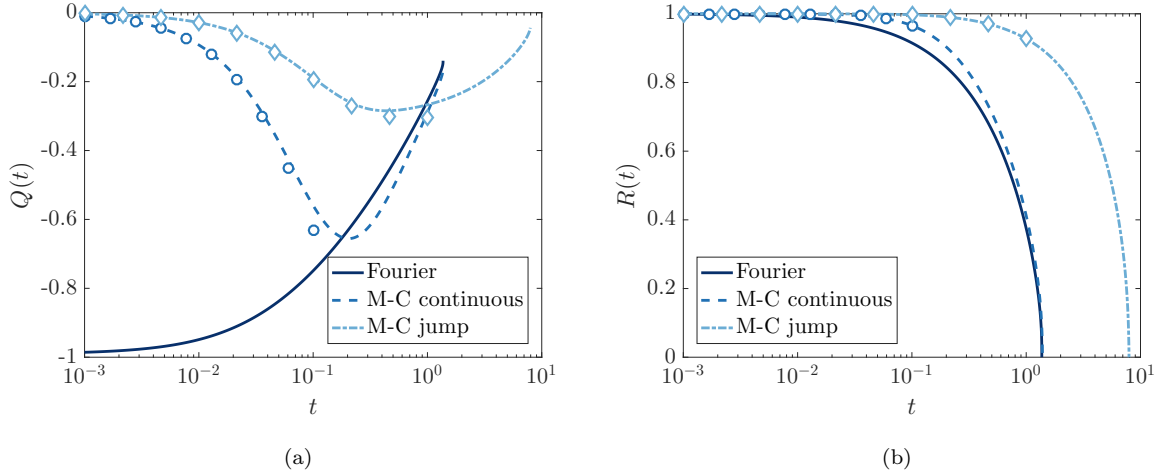


**Figure 2:** Comparison of melting dynamics obtained using Fourier’s law (solid lines), the Maxwell–Cattaneo equation with temperature continuity at the melt front (dashed lines), and the Maxwell–Cattaneo equation with a temperature jump at the melt front (dashed-dotted lines). (a) Evolution of the mean thermal flux defined by (47). (b) Evolution of the position of the melt front. Parameter values are  $R_0 = 10$  nm,  $\tau_r = 10^{-13}$  s and  $\beta = 0.25$ , corresponding to  $\gamma \simeq 0.10$  and  $\Delta T \simeq 873$  K. Circles and diamonds denote the asymptotic solutions as  $\gamma \rightarrow 0$  given by (39) and (43), respectively.

the evolution of the system on  $O(\gamma)$  time scales. As predicted by the asymptotic analysis, Fourier’s law leads to the mean thermal flux instantaneously obtaining the value of  $Q = -1$  and then monotonically decreasing in magnitude. When the Maxwell–Cattaneo equation is used, the magnitude of the flux grows exponentially with time from its initial value of zero until it reaches a maximum and begins to decay. The location of the maximum marks the transition to the diffusion-dominated transport regime. When the temperature is continuous across the melt front, the flux converges to the Fourier solution. Conversely, when there is a temperature jump across the melt front, the flux never approaches the Fourier solution. The different behaviour of the thermal flux can be rationalised in terms of the temperature at the melt front. Imposing the jump condition leads to the temperature at the melt front being larger than the Gibbs–Thomson melting temperature. Consequently, there is a smaller temperature difference between the liquid and the environment and the transfer of heat into the nanoparticle is reduced. This means that less thermal energy is transported to the melt front, resulting in a substantially slower melting process, as shown in Fig. 2 (b). In particular, the melting time, *i.e.*, the time required to completely melt the nanoparticle, is an order of magnitude larger in the jump-based Maxwell–Cattaneo model than in the corresponding continuity-based model.

The results of our analysis highlight two key shortcomings of the jump condition for the temperature. Firstly, unrealistically large temperature differences (or external temperatures) are required to initiate melting. Secondly, it is not possible to recover the classical, Fourier-based solution in the limit as the effective relaxation parameter tends to zero. These two shortcomings ultimately stem from the large change in interfacial temperature that occurs as a result of the thermal conductivity of the solid being greater than that of the liquid. In previous studies that model phase change with the Maxwell–Cattaneo equation and use the temperature jump condition [34, 35, 38], the thermal conductivities of the liquid and solid are assumed to be equal, thus avoiding the shortcomings that are observed here. Greenberg

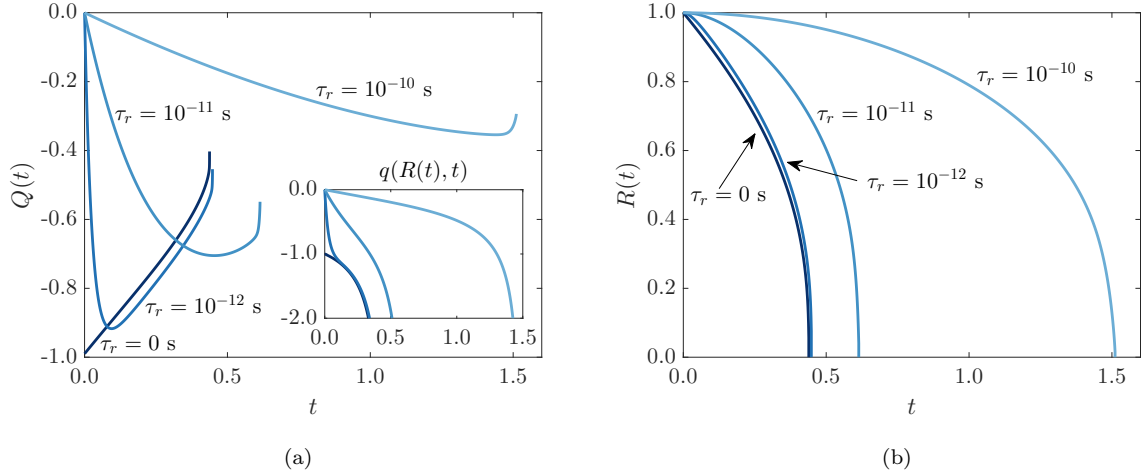


**Figure 3:** Influence of the relaxation time  $\tau_r$  on nanoparticle melting in the case of temperature continuity across the melt front. (a) Evolution of the mean flux (main panel) and flux at the melt front (inset). (b) Evolution of the position of the melt front. Parameter values are  $R_0 = 10$  nm and  $\beta = 10$  ( $\Delta T \simeq 22$  K).

[35] even states that it is the jump condition, not the continuity condition, that leads to solutions that are in agreement and consistent with those obtained using Fourier’s law. However, our asymptotic and numerical analyses show that this statement is simply not true. We believe that our results provide sufficient evidence to invalidate the jump condition. Thus, we will exclusively focus on the case of a continuous temperature profile throughout the remainder of this section.

We now explore how the thermal relaxation time affects the melting process for a fixed set of parameter values. We take  $R_0 = 10$  nm and  $\beta = 10$ , corresponding to  $\Delta T \simeq 22$  K, and examine values of  $\tau_r$  that range from  $10^{-12}$  s to  $10^{-10}$  s. For this value of  $\Delta T$ , the jump condition does not result in nanoparticle melting. The effective relaxation parameter  $\gamma$  lies between 0.025 and 2.5. The results of numerical simulations carried out with these parameters, along with the case when  $\tau_r = 0$ , are shown in Fig. 3. When  $\tau_r = 10^{-12}$  s ( $\gamma \simeq 0.025$ ), the evolution of the mean thermal flux can clearly be divided into the relaxation- and diffusion-dominated time regimes discussed in Section 4.1.2. As the thermal relaxation time is increased, the duration of the first, relaxation-dominated time regime is prolonged. In the case of  $\tau_r = 10^{-10}$  s, the nanoparticle completely melts before the second, diffusion-dominated regime is entered. Although the magnitude of the mean flux for  $\tau_r = 10^{-12}$  s and  $10^{-11}$  s eventually exceeds the Fourier flux, the inset of Fig. 3 (a) shows that Fourier’s law leads to the largest flux (in magnitude) at the melt front for all times. Thermal relaxation therefore inhibits the transport of thermal energy to the melt front, leading to slower melting kinetics and a melting time that monotonically increases with the relaxation time.

The size of the nanoparticle  $R_0$  influences the melting dynamics in a non-trivial manner. This is demonstrated in Fig. 4, which shows the results of numerical simulations carried out using larger nanoparticles, of radius  $R_0 = 100$  nm, and relaxation times in the range of  $10^{-11}$  s to  $10^{-9}$  s. The Stefan number was held at  $\beta = 10$ . This choice of parameters leads to the same values of the effective relaxation parameter  $\gamma$  considered in Fig. 3 for 10 nm nanoparticles, but it increases the Nusselt number by a factor of ten to  $\mathcal{N} \simeq 15.7$ . Figure 4 reveals that: (i) thermal relaxation can lead to a faster melting process, (ii) the melting time is a non-monotonic function of the relaxation time, and (iii)

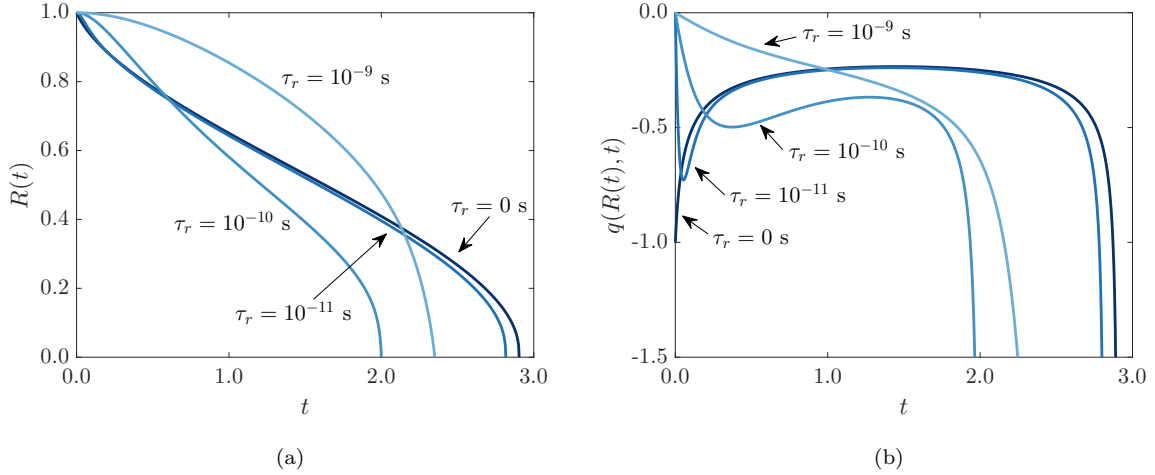


**Figure 4:** Influence of the relaxation time  $\tau_r$  on nanoparticle melting in the case of temperature continuity across the melt front. Evolution of the position of the melt front (a) and mean flux (b). Parameter values are  $R_0 = 100$  nm and  $\beta = 10$  ( $\Delta T \simeq 22$  K).

the thermal flux at the melt front can be a non-monotonic function of time. These three features are attributed to the competing roles of rapid heat transfer, as characterised by the large Nusselt number, and thermal relaxation. In the case of zero relaxation time, the thermal flux at the melt front (Fig. 4 (b)) initially decreases in magnitude. This is due to the sudden increase in surface temperature, which, in turn, reduces the driving force behind heat exchange with the environment. In systems with non-zero relaxation time, the sharp increase in surface temperature is dampened by relaxation effects, allowing the magnitude of the flux at the melt front to overshoot and subsequently exceed the Fourier value, leading to a melting process that is faster overall. However, the time at which the overshoot occurs increases with the relaxation time. For sufficiently large values of the relaxation time, no overshoot occurs at all, and the melting time becomes larger compared to the Fourier case. As  $\tau_r$  is increased from zero, we find that the melting time decreases until a critical value given by  $\tau_r \simeq 2.25 \times 10^{-10}$  s is reached, after which the melting time begins to increase with the relaxation time. In the case of the 10 nm nanoparticles considered in Fig. 3, heat is transported away from the surface sufficiently quickly that large increases in temperature and hence decreases in the magnitude of the flux are avoided.

The temperature profiles obtained from Fourier and Maxwell–Cattaneo models are compared in Fig. 5. The parameter values are  $R_0 = 10$  nm,  $\beta = 10$ , and  $\tau_r = 10^{-10}$  s and correspond to those of Fig. 3. To facilitate comparing the models, the evolution of the temperature is described in terms of the thickness of the liquid region, given by  $1 - R(t)$ . For a large part of the melting process, the temperature profiles, for a given liquid thickness, are quantitatively similar. However, key discrepancies arise near the end of the melting process, when the radius of the solid core becomes small. Figure 5 (b) shows the development of a local maximum in the temperature profile in the case of Maxwell–Cattaneo conduction, a feature which is impossible in Fourier-based heat conduction. Despite the non-monotonic temperature profile, the thermal flux (not shown) remains negative, implying there are regions where heat flows in the direction of positive temperature gradients. As will be discussed below, such behaviour is non-physical and violates the second law of thermodynamics. The underlying mechanism for this non-physical behaviour is the finite speed of heat propagation which is fundamental to the Maxwell–Cattaneo

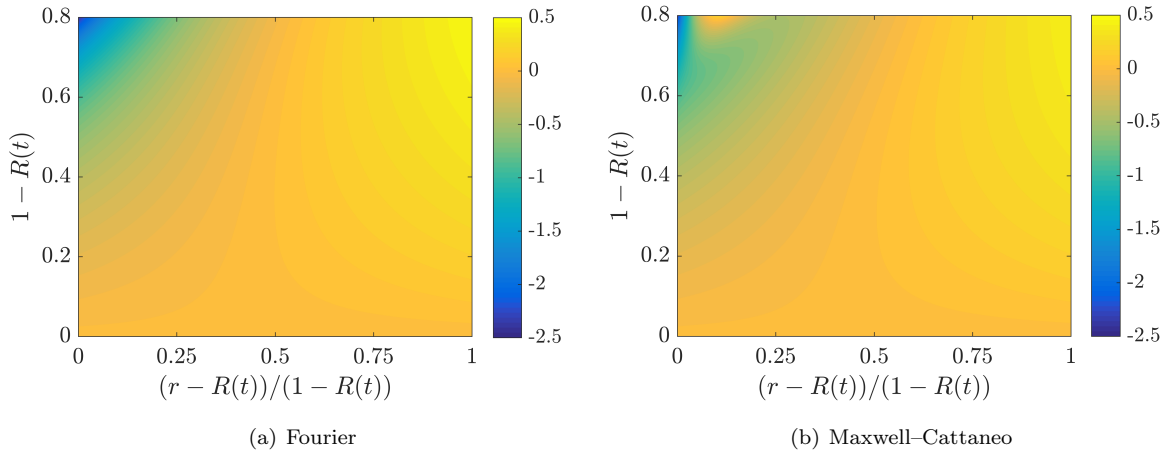


**Figure 5:** Evolution of the temperature profile in the case of Fourier conduction (a) and Maxwell-Cattaneo conduction (b). To facilitate making a comparison between the models, the evolution is described in terms of the width of the liquid region  $1 - R(t)$ . Temperature continuity was assumed when simulating the model with the Maxwell-Cattaneo equation. Parameter values match those of Fig. 3:  $R_0 = 10$  nm and  $\beta = 10$ . A value of  $\tau_r = 10^{-10}$  s was used in panel (b).

equation. In dimensionless terms, the speed of heat propagation can be expressed as  $v = \sqrt{\beta/(\gamma\mathcal{N})}$  and, for this set of parameter values, evaluates to  $v \simeq 1.6$ . The speed of the melt front monotonically increases from zero, eventually exceeding the speed of heat propagation when  $t \simeq 1.4$ . After this time, the melting front propagates faster than thermal energy can be delivered to it. The system responds by introducing a local maximum in the temperature, amplifying the local temperature gradient and flux, thus compensating for the insufficient rate of thermal transport from the outer boundary.

For small temperature differences  $\Delta T$  and hence large Stefan numbers, the asymptotically reduced model (49) can be used to describe nanoparticle melting. In Fig. 6, numerical results obtained from the full model (16)–(22) are compared to those of the reduced model (49). The Stefan number is set to  $\beta = 50$ , corresponding to  $\Delta T \simeq 4.4$  K, and a relaxation time of  $\tau_r = 10^{-10}$  s is used. Various nanoparticle radii are considered. The position of the melt front and the mean flux are plotted in Fig. 6 as functions of the dimensional time rather than the dimensionless time because the time scale that is used to non-dimensionalise the model contains a factor of  $R_0$  and therefore varies between simulations. From Fig. 6 (a), the initial behaviour of the mean flux is seen to be independent of the size of the nanoparticle, which can be verified by re-dimensionalising the small-time solution for the thermal flux (32b), yielding  $q_l \sim (h\Delta T)(t/\tau_r)$ . The difference in the long-time behaviour of the flux is attributed to the varying size of the effective relaxation parameter  $\gamma$ . We find that  $\gamma = 0.50, 0.10$ , and  $0.050$  for 10 nm, 50 nm, and 100 nm nanoparticles, respectively. The relatively strong influence of thermal relaxation in 10 nm nanoparticles prevents the second, diffusion-dominated regime of transport from being reached before the solid core is completely transformed into liquid. For all nanoparticle radii, there is excellent agreement between the asymptotically reduced model and the full model.

The role of thermal relaxation in nanoparticles composed of gold and lead can be studied using the parameter values in Table 1. The maximum value of the heat transfer coefficient for each material can be calculated using the method outlined by Ribera and Myers [21]. We find that  $h_{\max}$  has the same order of magnitude for each material. For the purpose of this discussion, it is sufficient to set  $h_{\max} = 4.9 \times$

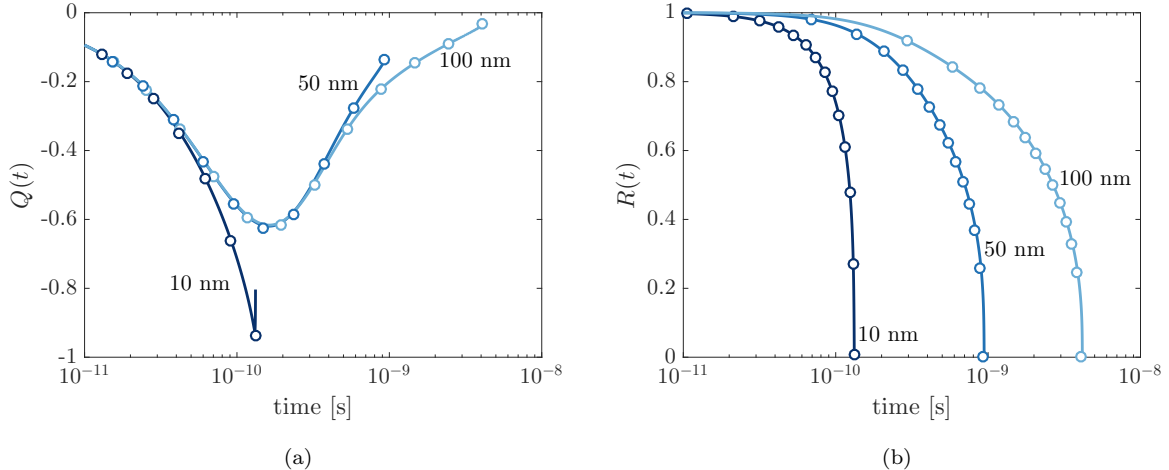


**Figure 6:** Comparison of the full model and the asymptotically reduced model for large Stefan numbers and various nanoparticle radii  $R_0$ . Lines denote numerical simulations of the full model (16)–(22) with temperature continuity imposed at the melt front. Symbols represent numerical simulations of the reduced model given by (49). (a) Evolution of the mean flux as defined in (47). (b) Evolution of the position of the solid-liquid interface. Parameter values are  $\beta = 50$ , corresponding to  $\Delta T \simeq 4.4$  K, and  $\tau_r = 10^{-10}$  s.

$10^9$  W/(m<sup>2</sup>·K) for each material. The melting times of tin, gold, and lead nanoparticles computed using Fourier’s law and the Maxwell–Cattaneo equation, along with their relative differences, are tabulated in Table 2 for various values of  $R_0$  and  $\Delta T$ . The relaxation time is fixed at  $\tau_r = 10^{-10}$  s. Thermal relaxation plays the strongest role in 10 nm nanoparticles that are subject to a 100 K temperature difference, as these conditions lead to the most rapid melting. As the radius of the nanoparticle increases or the temperature difference decreases, both of which lead to a longer melting process, the difference in the Fourier and Maxwell–Cattaneo melting times decreases, implying thermal relaxation plays a weaker role. For each value of  $\Delta T$  and  $R_0$ , the relative difference in melting time is similar across the materials, indicating that thermal relaxation affects each material in roughly the same way. Thus, the results of this section, which are based on parameter values associated with tin, are likely to hold for other materials as well.

Finally, we address one of the major criticisms of the Maxwell–Cattaneo equation, which is that it can lead to negative entropy production, in violation of the second law of thermodynamics. The dimensionless entropy generation  $\dot{S}$  can be written as [28]

$$\dot{S} = -\frac{q}{[\theta(1-\ell) + T]^2} \frac{\partial T}{\partial r}. \quad (51)$$

Thus, positive entropy generation requires thermal energy to travel in the direction of negative temperature gradient. The onset of a local maximum in the temperature profile observed in Fig. 5 (b) leads to a region of negative entropy production and a breakdown of the model. However, this breakdown occurs late in the melting process, when the radius of the solid core has decreased to roughly 20% of its initial value. In dimensional terms, this corresponds to a radius of 2 nm. On such length scales, the validity of the continuum approximation also comes into question. Up to this point, the Maxwell–Cattaneo equation provides a thermodynamically consistent description of nanoparticle melting. Determining explicit conditions that guarantee positive entropy production is difficult. In the case of a large Stefan number,

**Table 2:** Dimensional melting times of tin, gold, and lead nanoparticles computed using Fourier’s law,  $t_F$ , and the Maxwell–Cattaneo equation,  $t_{MC}$ , for various radii  $R_0$  and temperature differences  $\Delta T$ . The relative difference between the melting times is defined as  $\eta = |t_F - t_{MC}|/t_F$ .

	$\Delta T = 1$ K			$\Delta T = 10$ K			$\Delta T = 100$ K		
10 nm	$t_F$ [ps]	$t_{MC}$ [ps]	$\eta$	$t_F$ [ps]	$t_{MC}$ [ps]	$\eta$	$t_F$ [ps]	$t_{MC}$ [ps]	$\eta$
Tin	110	248	1.26	30.4	88.4	1.91	5.50	30.1	4.46
Gold	99.6	272	1.73	35.2	121	2.43	7.17	41.6	4.81
Lead	54.7	166	2.03	19.1	67.6	2.54	4.43	26.7	5.04
100 nm	$t_F$ [ns]	$t_{MC}$ [ns]	$\eta$	$t_F$ [ns]	$t_{MC}$ [ns]	$\eta$	$t_F$ [ns]	$t_{MC}$ [ns]	$\eta$
Tin	12.2	12.0	0.011	2.25	1.94	0.139	0.329	0.230	0.300
Gold	6.73	6.86	0.018	1.71	1.65	0.038	0.273	0.242	0.113
Lead	9.75	9.61	0.015	2.21	1.87	0.155	0.372	0.279	0.250

however, it is straightforward to show that the asymptotically reduced model (49) will always produce entropy, therefore ensuring the second law of thermodynamics is satisfied during the melting process.

## 6 Conclusions

The melting of spherical nanoparticles is studied using a non-classical model of heat conduction, based on the Maxwell–Cattaneo equation, that accounts for the finite thermal relaxation time of materials. By seeking asymptotic and numerical solutions to the model using realistic parameter values, we show that the jump boundary condition for the temperature produces non-physical results. In particular, the jump condition leads to an effective nanoparticle melting temperature that is much greater than the bulk melting temperature, which contradicts the findings of several experimental studies. Furthermore, it is not generally possible to recover the Fourier-based solution from the Maxwell–Cattaneo model when the jump condition is imposed. Our results highlight important inadequacies in the jump condition and demonstrate that it is not appropriate to use in models of phase change that are based on the Maxwell–Cattaneo equation. Similar considerations may be required for other non-Fourier conduction laws as well.

By analysing the model with temperature continuity imposed across the melt front, we find there is a non-trivial interplay between heat exchange with the environment and thermal relaxation. Depending on the size of the nanoparticle, thermal relaxation can either decelerate or accelerate the overall melting process relative to the case of Fourier conduction. The relevance of thermal relaxation generally increases as the nanoparticle radius decreases or the imposed temperature difference increases, both of which lead to melting processes that occur more rapidly. For the parameter range and materials considered here, thermal relaxation is found to modify the melting time by up to 500%. We can conclude that thermal relaxation is an important process to capture in models of nanoparticle melting and will likely influence the dynamics of phase change in other technologically relevant systems as well.

A key shortcoming of the proposed model is that it can violate the second law of thermodynamics and lead to negative production of entropy. Numerical simulations show that negative entropy production occurs when the speed of the melt front exceeds the finite speed of heat propagation. Such behaviour is only expected to take place near the end of the melting process when the radius of the solid core

becomes a few nanometers in size. Until this point, the Maxwell–Cattaneo equation is able to provide a thermodynamically consistent description of nanoscale heat transport. Future studies of nanoparticle melting can explore using alternative models of non-Fourier heat conduction to avoid the issue of negative entropy production altogether.

## Acknowledgements

The authors thank Brian Wetton and Sonia Fernandez-Mendez for helpful discussions regarding the numerical solution of the governing equations. This project has received funding from the European Union’s Horizon 2020 research and innovation programme under grant agreement No 707658. MC acknowledges that the research leading to these results has received funding from ‘la Caixa’ Foundation. TM acknowledges financial support from the Ministerio de Ciencia e Innovación grant MTM2017-82317-P. The authors have been partially funded by the CERCA Programme of the Generalitat de Catalunya.

## References

- [1] D. G. Cahill, W. K. Ford, K. E. Goodson, G. D. Mahan, A. Majumdar, H. J. Maris, R. Merlin, and S. R. Phillpot. Nanoscale thermal transport. *J. Appl. Phys.*, 93(2):793–818, 2003.
- [2] D. G. Cahill, P. V. Braun, G. Chen, D. R. Clarke, S. Fan, K. E. Goodson, P. Keblinski, W. P. King, G. D. Mahan, A. Majumdar, H. J. Maris, S. R. Phillpot, E. Pop, and L. Shi. Nanoscale thermal transport. ii. 2003–2012. *Appl. Phys. Rev.*, 1(1):011305, 2014.
- [3] T. C. Yih and M. Al-Fandi. Engineered nanoparticles as precise drug delivery systems. *J. Cell. Biochem.*, 97:1184–1190, 2006.
- [4] J. A. Dieringer, A. D. McFarland, N. C. Shah, D. A. Stuart, A. V. Whitney, C. R. Yonzon, M. A. Young, X. Zhang, and R. P. Van Duyne. Introductory Lecture: Surface enhanced Raman spectroscopy: New materials, concepts, characterization tools, and applications. *Faraday Discuss.*, 132:9–26, 2006.
- [5] F. Gröhn, G. Kim, B. J. Bauer, and E. J. Amis. Nanoparticle formation within dendrimer-containing polymer networks: Route to new organic-inorganic hybrid materials. *Macromolecules*, 34:2179–2185, 2001.
- [6] V. Cregan and T. G. Myers. Modelling the efficiency of a nanofluid direct absorption solar collector. *Int. J. Heat Mass Tran.*, 90:505–514, 2015.
- [7] P. Buffat and J. P. Borel. Size effect on the melting temperature of gold particles. *Phys. Rev. A*, 13(6):2287, 1976.
- [8] T. B. David, Y. Lereah, G. Deutscher, R. Kofman, and P. Cheyssac. Solid-liquid transition in ultra-fine lead particles. *Philos. Mag. A*, 71(5):1135–1143, 1995.
- [9] C. R. M. Wronski. The size dependence of the melting point of small particles of tin. *Brit. J. Appl. Phys.*, 18(12):1731, 1967.

- [10] S. L. Lai, J. Y. Guo, V. Petrova, G. Ramanath, and L. H. Allen. Size-dependent melting properties of small tin particles: nanocalorimetric measurements. *Phys. Rev. Lett*, 77(1):99, 1996.
- [11] M. Zhang, M. Y. Efremov, F. Schiettekatte, E. A. Olson, A. T. Kwan, S. L. Lai, T. Wisleder, J. E. Greene, and L. H. Allen. Size-dependent melting point depression of nanostructures: nanocalorimetric measurements. *Phys. Rev. B*, 62(15):10548, 2000.
- [12] J. Sun and S. L. Simon. The melting behavior of aluminum nanoparticles. *Thermochim. Acta*, 463(1):32–40, 2007.
- [13] R. C. Tolman. The effect of droplet size on surface tension. *J. Chem. Phys.*, 17(3):333–337, 1949.
- [14] D. D. Joseph and L. Preziosi. Heat waves. *Rev. Mod. Phys.*, 61:41–73, 1989.
- [15] D. D. Joseph and L. Preziosi. Addendum to the paper “Heat waves”. *Rev. Mod. Phys.*, 62:375–391, 1990.
- [16] J. M. Back, S. W. McCue, and T. J. Moroney. Including nonequilibrium interface kinetics in a continuum model for melting nanoscaled particles. *Sci. Rep.*, 4, 2014.
- [17] F. Font and T. G. Myers. Spherically symmetric nanoparticle melting with a variable phase change temperature. *J. Nanopart. Res.*, 15(12):2086, 2013.
- [18] F. Font, T. G. Myers, and S. L. Mitchell. A mathematical model for nanoparticle melting with density change. *Microfluid. Nanofluid.*, 18(2):233–243, 2015.
- [19] S. W. McCue, B. Wu, and J. M. Hill. Micro/nanoparticle melting with spherical symmetry and surface tension. *IMA J. Appl. Math.*, 74(3):439–457, 2009.
- [20] T. G. Myers and F. Font. On the one-phase reduction of the Stefan problem with a variable phase change temperature. *Int. Commun. Heat Mass*, 61:37–41, 2015.
- [21] H. Ribera and T. G. Myers. A mathematical model for nanoparticle melting with size-dependent latent heat and melt temperature. *Microfluid. Nanofluid.*, 20(11):147, 2016.
- [22] T. G. Myers. Mathematical modelling of phase change at the nanoscale. *Int. Commun. Heat Mass*, 76:59–62, 2016.
- [23] V. Peshkov. Determination of the velocity of propagation of the second sound in helium ii. *J. Phys. USSR*, 10:389–398, 1946.
- [24] C. Cattaneo. A form of heat conduction equation which eliminates the paradox of instantaneous propagation. *Compte Rendus*, 247(4):431–433, 1958.
- [25] P. Vernotte. Les paradoxes de la theorie continue de l’equation de la chaleur. *Comptes Rendus de l’Academie des Sciences*, 246(22):3154–3155, 1958.
- [26] J. C. Maxwell. On the dynamical theory of gases. *Philosophical Transactions of the Royal Society of London*, 157:49–88, 1867.
- [27] M. Chester. Second sound in solids. *Phys. Rev.*, 131(5):2013, 1963.

- [28] T. J. Bright and Z. M. Zhang. Common misperceptions of the hyperbolic heat equation. *J. Thermophys. Heat Tr.*, 23:601–607, 2009.
- [29] D. Jou, J. Casas-Vázquez, and G. Lebon. *Extended Irreversible Thermodynamics*. Springer, fourth edition, 2010.
- [30] P. Ván and T. Fülöp. Universality in heat conduction theory: weakly nonlocal thermodynamics. *Ann. Phys.*, 524(8):470–478, 2012.
- [31] P. Colli and M. Grasselli. Hyperbolic phase change problems in heat conduction with memory. *Proc. Roy. Soc. Edinb. A*, 123(3):571–592, 1993.
- [32] A. Friedman and B. Hu. The Stefan problem for a hyperbolic heat equation. *J. Math. Anal. Appl.*, 138(1):249–279, 1989.
- [33] R. E. Showalter and N. J. Walkington. A hyperbolic Stefan problem. *Q. Appl. Math.*, 45(4):769–781, 1987.
- [34] D. E. Glass, M. Necati Ozisik, S. S. McRae, and W. S. Kim. Formulation and solution of hyperbolic Stefan problem. *J. Appl. Phys.*, 70(3):1190–1197, 1991.
- [35] J. M. Greenberg. A hyperbolic heat transfer problem with phase changes. *IMA J. Appl. Math.*, 38(1):1–21, 1987.
- [36] A. D. Solomon, V. Alexiades, D. G. Wilson, and J. Drake. On the formulation of hyperbolic Stefan problems. *Q. Appl. Math.*, 43(3):295–304, 1985.
- [37] S. L. Sobolev. Transport processes and traveling waves in systems with local nonequilibrium. *Phys. Usp.*, 34(3):217, 1991.
- [38] S. L. Sobolev. The local-nonequilibrium temperature field around the melting and crystallization front induced by picosecond pulsed laser irradiation. *Int. J. Thermophys.*, 17(5):1089–1097, 1996.
- [39] M. H. Sadd and J. E. Didlake. Non-Fourier melting of a semi-infinite solid. *J. Heat Transf.*, 99(1):25–28, 1977.
- [40] H. Liu, M. Bussmann, and J. Mostaghimi. A comparison of hyperbolic and parabolic models of phase change of a pure metal. *Int. J. Heat Mass Tran.*, 52(5):1177–1184, 2009.
- [41] A. M. Mullis. Rapid solidification within the framework of a hyperbolic conduction model. *Int. J. Heat Mass Tran.*, 40(17):4085–4094, 1997.
- [42] G.-X. Wang and V. Prasad. Microscale heat and mass transfer and non-equilibrium phase change in rapid solidification. *Mat. Sci. Eng. A-Struc.*, 292(2):142–148, 2000.
- [43] Z.-S. Deng and J. Liu. Non-Fourier heat conduction effect on prediction of temperature transients and thermal stress in skin cryopreservation. *J. Therm. Stresses*, 26(8):779–798, 2003.
- [44] H. Ahmadikia and A. Moradi. Non-Fourier phase change heat transfer in biological tissues during solidification. *Heat Mass Transfer*, 48(9):1559–1568, 2012.

- [45] A. Kumar, S. Kumar, V. K. Katiyar, and S. Telles. Phase change heat transfer during cryosurgery of lung cancer using hyperbolic heat conduction model. *Comput. Biol. Med.*, 84:20–29, 2017.
- [46] M. G. Hennessy, M. Calvo-Schwarzwalder, and T. G. Myers. Asymptotic analysis of the Guyer-Krumhansl-Stefan model for nanoscale solidification. *Applied Mathematical Modelling*, 2018.
- [47] V. Alexiades and A. D. Solomon. *Mathematical Modeling Of Melting And Freezing Processes*. Hemisphere, 1993.
- [48] V. A. Cimmelli, D. Jou, and A. Sellitto. Propagation of temperature waves along core-shell nanowires. *J. Non-Equil. Thermody.*, 35(3):267–278, 2010.
- [49] D. Jou, V. A. Cimmelli, and A. Sellitto. Nonequilibrium temperatures and second-sound propagation along nanowires and thin layers. *Phys. Lett. A*, 373(47):4386–4392, 2009.
- [50] T G Myers, M M MacDevette, F Font, and V Cregan. Continuum mathematics at the nanoscale. *J. Math. Ind.*, 4(1), 2014.
- [51] T. Bachelis, H.-J. Guntherodt, and R. Schafer. Melting of isolated tin nanoparticles. *Phys. Rev. Lett.*, 85(6):1250, 2000.
- [52] H. Jiang, K.-S. Moon, H. Dong, F. Hua, and C. P. Wong. Size-dependent melting properties of tin nanoparticles. *Chem. Phys. Lett.*, 429(4-6):492–496, 2006.
- [53] A. Rieth, R. Kovacs, and T. Fulop. Implicit numerical schemes for generalized heat conduction equations. *arXiv preprint arXiv:1805.01108*, 2018.
- [54] M. Takagi. Electron-diffraction study of liquid-solid transition of thin metal films. *J. Phys. Soc. Jpn.*, 9(3):359–363, 1954.
- [55] Qingshan Fu, Yongqiang Xue, Zixiang Cui, and Huijuan Duan. Research into the rationality and the application scopes of different melting models of nanoparticles. *J. Nanopart. Res.*, 19(7):263, 2017.